Supporting Information

Modulating $CsPbBr_3$ nanocrystals encapsulated in PCN-224(Zr) for boosting full-spectrum-driven CO_2 reduction: S-scheme transfer, photothermal-synergistic effect and DFT calculations

Yan-He Chen[a], Jin-Qiu Shen[a], Xiao-Lu Chen[a], Luobing Tang[b], Na Zhang[b], Jian-Yong Zhang [a,*], and Zhen-Jiang Liu[a,*]

[a] School of Chemical and Environmental Engineering, Shanghai Institute of Technology, Shanghai 201418, P.R.China

[b] School of Materials Science and Engineering, Shanghai Institute of Technology, Shanghai 201418, P.R.China

**Dr. Jian-Yong Zhang, E-mail: jianyong1106@163.com;*

Prof. Zhen-Jiang Liu, E-mail:zjliu@sit.edu.cn

List of Contents

Fig.S20 The high-resolution XPS spectra of C 1s (a) and O 1s (b) over PCN-224(Zr) and $CsPbBr_3$@PCN-224(Zr)-10 composite.

Fig.S21 The in situ XPS spectra of Br 3d (a) and Cs 3d (b) over $CsPbBr_3$@PCN-224(Zr)-10 composite with/without light irradiation.

Fig.S22 The proposed mechanism of photocatalytic CO_2RR process.

3. Supplementary Tables

Table S1 The fitted internal resistance (R_s) and charge transfer resistance (R_{ct}) from the Nyquist plots.

Table S2 Summary of the photocatalytic CO_2RR performance under vis-NIR irradiation for 4 h over different photocatalysts in this paper.

Table S3 Comparison of the photocatalytic CO_2 reduction over related photocatalysts.

Table S4 The fitted parameters of time-resolved PL curves of five photocatalysts.

4. References

1. Experimental

1.1 Characterization

The Fourier transform infrared (FT-IR) spectroscopy in the range of 500 cm^{-1}-4000 cm^{-1} was recorded on a Nicolet NEXUS 670 spectrophotometer. The crystal structure was determined by powder X-ray diffraction (PXRD) on a Rigaku D/Max-2500 diffractometer for a Cu Kα radiation (λ = 1.5418 Å). TGA was performed under flowing N_2 atmosphere using a Mettler Toledo TGA/SDTA851 instrument. The morphology was studied by scanning electron microscopy (SEM) (S-4800 II microscope, Hitachi), transmission electron microscopy (TEM) and high resolution transmission electron microscopy (HRTEM) (FEI JEM-2100). X-ray photoelectron spectroscopy (XPS) was obtained on Physical Electronics PHI-5702 with Al Kα excitation. The UV-vis diffuse reflectance spectra (UV-vis DRS) were obtained by Agilent Cary 5000 spectrophotometer. The steady-state photoluminescence (PL) spectra and TRPL spectra were studied on the Varian Cary Eclipse spectrometer (Hitachi F-7000). Transient surface photovoltage (TPV) spectra were conducted on a CEL-TPV2000 instrument (Beijing China Education Au-light Co., Ltd., China).

1.2 Photo-electrochemical measurements

The photo-electrochemical measurements (including photocurrent, linear sweep voltammetry, electrochemical impedance spectroscopy) were carried out on a CHI-660D electrochemical station (Chenhua Instrument, China) in a conventional standard three-electrode cell. An Ag/AgCl electrode was used as the reference electrode, the Pt wire as the counter electrode and the $CsPbBr_3$ QDs, PCN-224(Zr) or $CsPbBr_3$@PCN-224-x composites were coated on FTO glass as the working electrode. A Xenon lamp (300 W, PLS-SXE300C, Beijing Perfect light Co. Ltd., China) equipped with different cut-off filter was utilized as simulated light source.

1.3 Evaluation of photocatalytic CO_2 reduction

The photocatalytic CO_2 reduction test was conducted on a photoreactor system (Beijing, Perfectlight Technology Co., Ltd.) as described in our previous study. Typically, as-prepared photocatalyst (4 mg) was dispersed in CH_3CN (30 mL) with 100 μL of DI water under continuous magnetic stirring. The reaction temperature was maintained at 20 °C by a temperature-controlled circulating low-temperature water flow. Firstly, the mixture was degassed and bubbled with high-purity CO_2 several times to remove the air inside and then was injected with high-purity CO_2. Then, the photoreactor was irradiated under a 300 W Xe lamp with different cutoff filter to simulate UV, vis-NIR and full-spectrum light, respectively. During the reaction process, the produced gaseous products were detected and quantified by gas chromatograph (GC-7890B, Agilent) equipped with a hydrogen flame ionization detector (FID) and a thermal conductivity detector (TCD). The cyclic experiments (4 h in each run) were carried out to evaluate the stability of the $CsPbBr_3$@PCN-224(Zr)-x composite. Between the runs, the reactor was degassed and refilled with high-purity CO_2. All the experiments were repeated twice and the data used in the paper was the average value.

2. Supplementary Figures

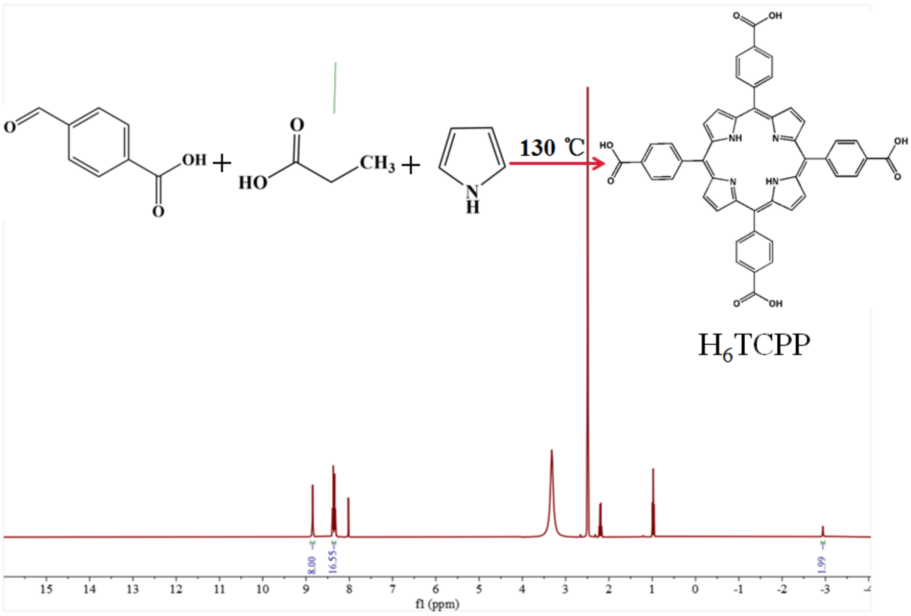

Fig.S1 The synthesis procedure and [1]HNMR spectra of as-synthesized H_6TCPP ligand.

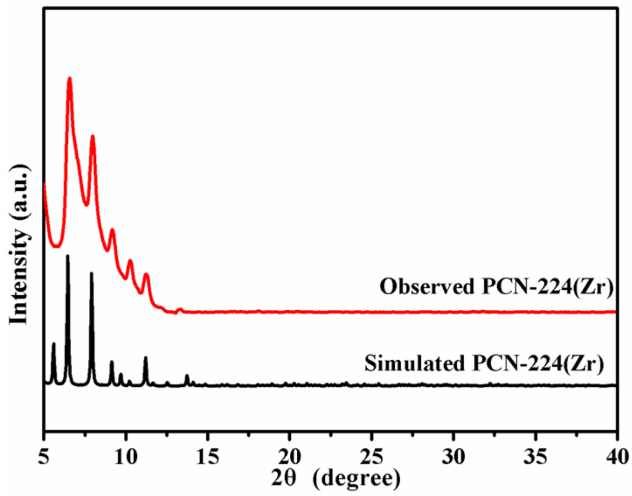

Fig.S2 The PXRD patterns of observed and simulated PCN-224(Zr).

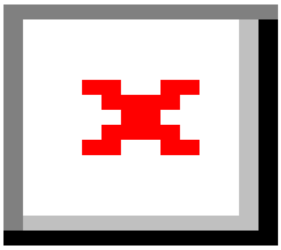

Fig.S3 The DTG curves of samples under air atmosphere.

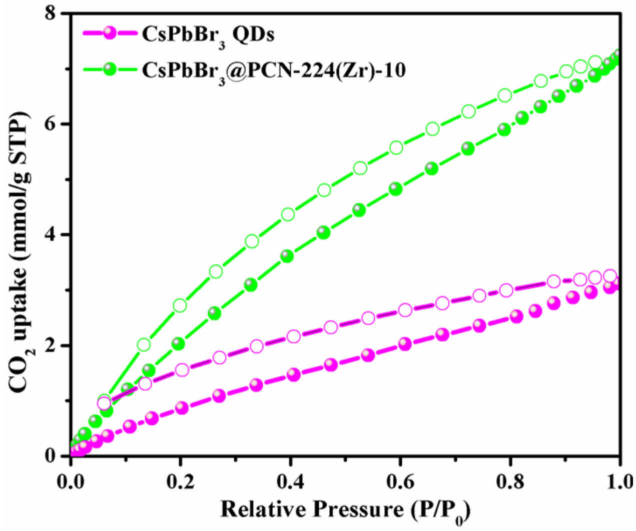

Fig.S4 The CO_2 adsorption isotherms of $CsPbBr_3$ QDs and $CsPbBr_3$@PCN-224(Zr)-10 composite at room temperature.

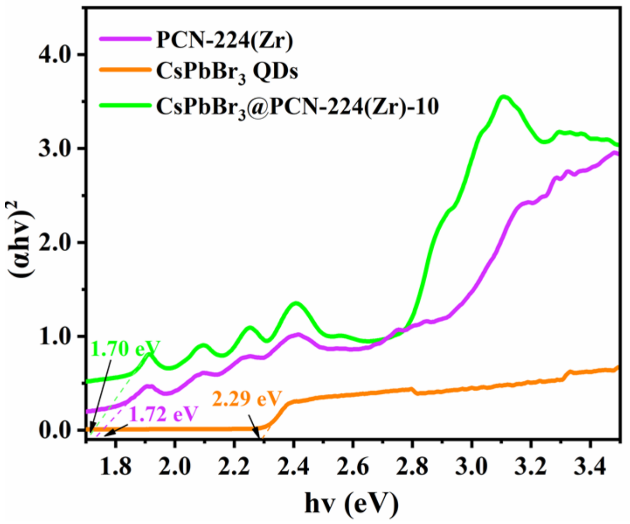

Fig.S5 The Tauc plots from UV-vis curves.

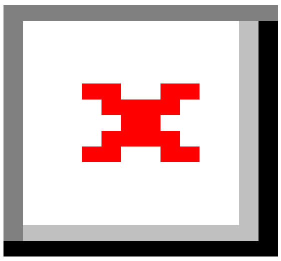

Fig.S6 The EIS plots of $CsPbBr_3$@PCN-224(Zr)-x composite with or without irradiation (x=5, 15).

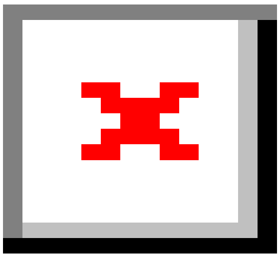

Fig.S7 The LSV curves with or without light irradiation for $CsPbBr_3$@PCN-224(Zr)-x photocatalysts (x=5 and 15).

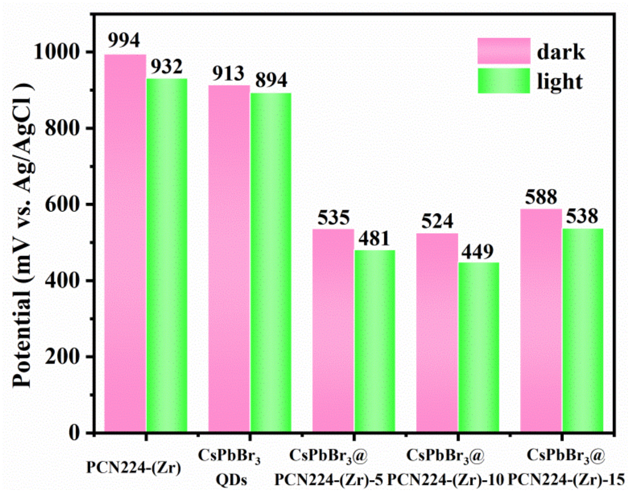

Fig.S8 The overpotentials of five photocatalysts with or without irradiation.

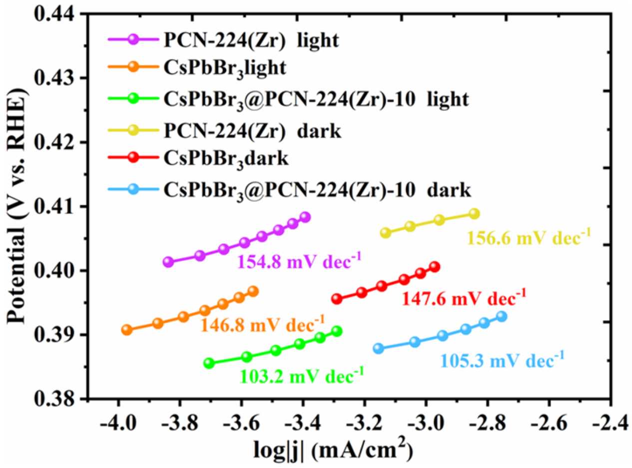

Fig.S9 The Tafel plots of PCN-224(Zr), $CsPbBr_3$ QDs, and $CsPbBr_3$@PCN-224(Zr)-

10 composite with or without irradiation.

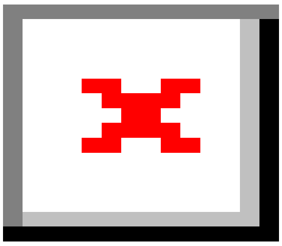

Fig.S10 The Tafel plots of $CsPbBr_3$@PCN-224(Zr)-x composite with or without irradiation (x=5, 15).

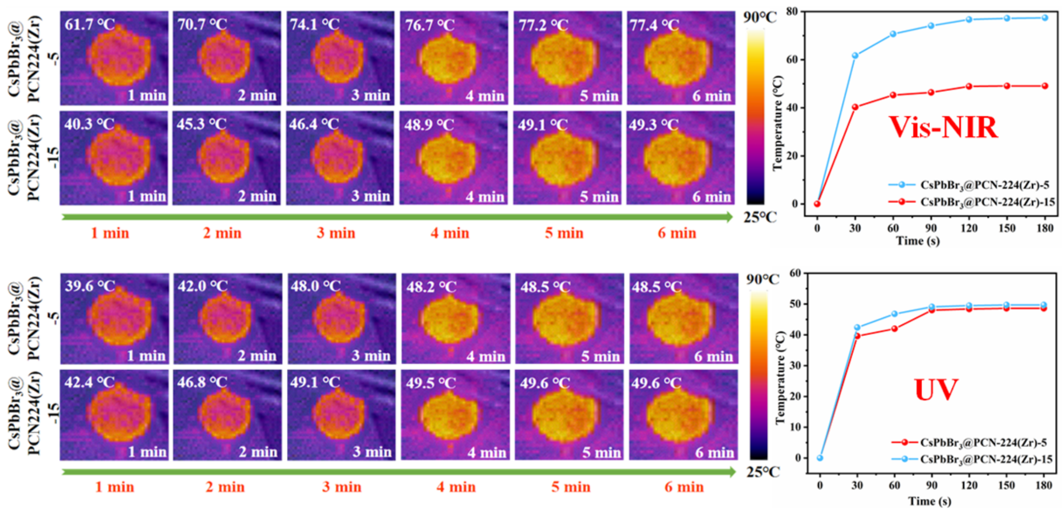

Fig.S11 Real-time thermal images of the solid $CsPbBr_3$@PCN-224(Zr)-5, and $CsPbBr_3$@PCN-224(Zr)-15 samples under vis-NIR and UV irradiations, respectively.

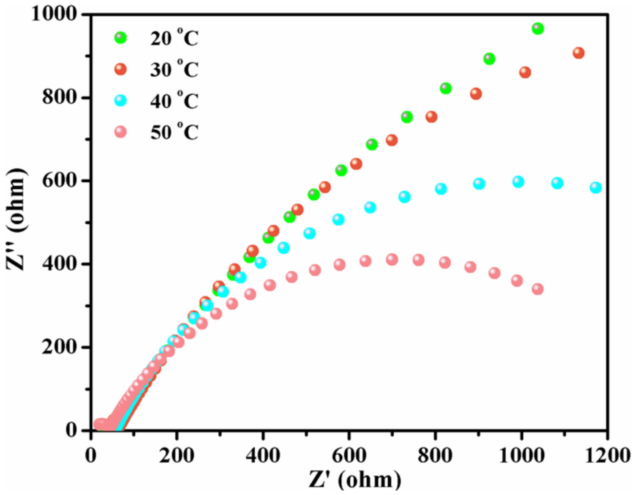

Fig.S12 The EIS plots of $CsPbBr_3$@PCN-224(Zr)-10 at different temperatures.

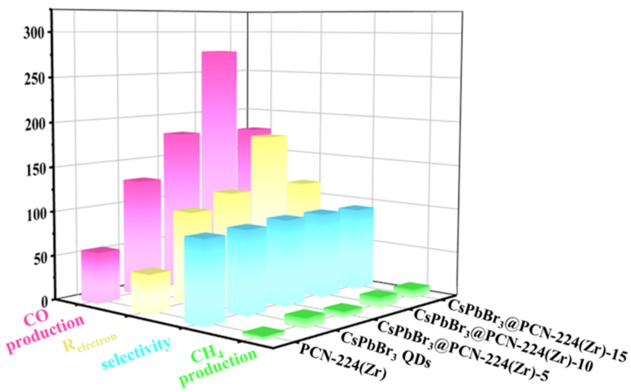

Fig.S13 The photocatalytic CO_2RR performances of the five catalysts under vis-NIR irradiation for 4 h.

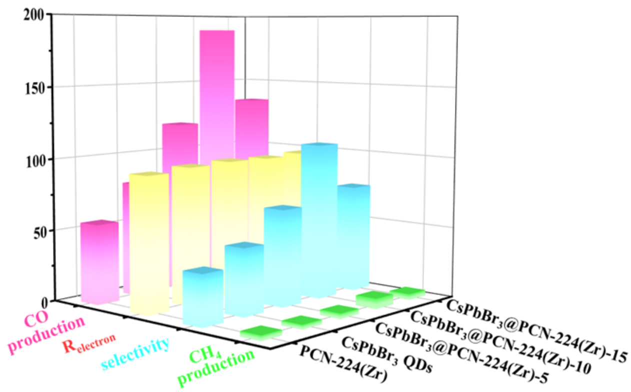

Fig.S14 The photocatalytic CO_2RR performances of the five catalysts under UV light irradiation for 4 h.

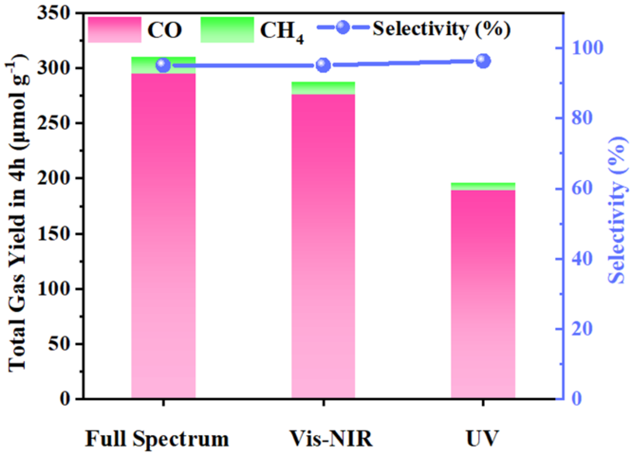

Fig.S15 The comparison of the photocatalytic CO_2RR activity over different light irradiation.

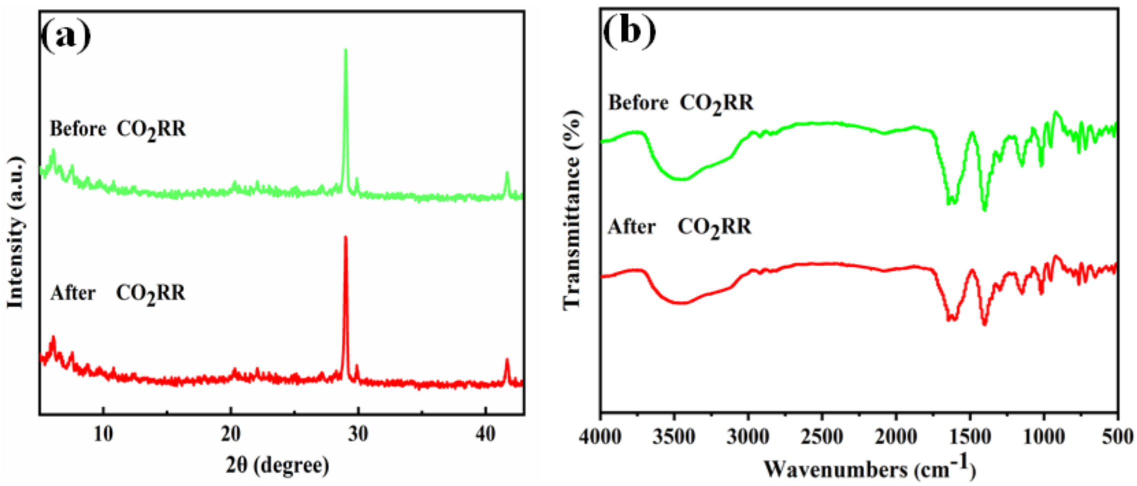

Fig.S16 The $CsPbBr_3$@PCN-224(Zr)-10 photocatalyst characterization after four cyclic CO_2RR runs: XRD (a), and FT-IR (b).

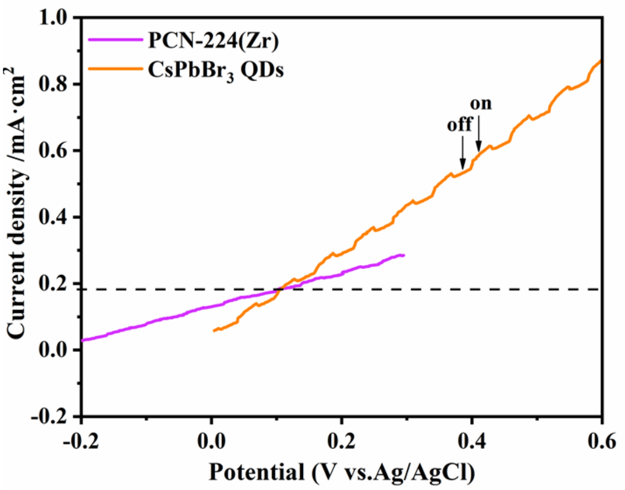

Fig.S17 The current-potential curves of PCN-224(Zr) and $CsPbBr_3$ under solar light irradiation.

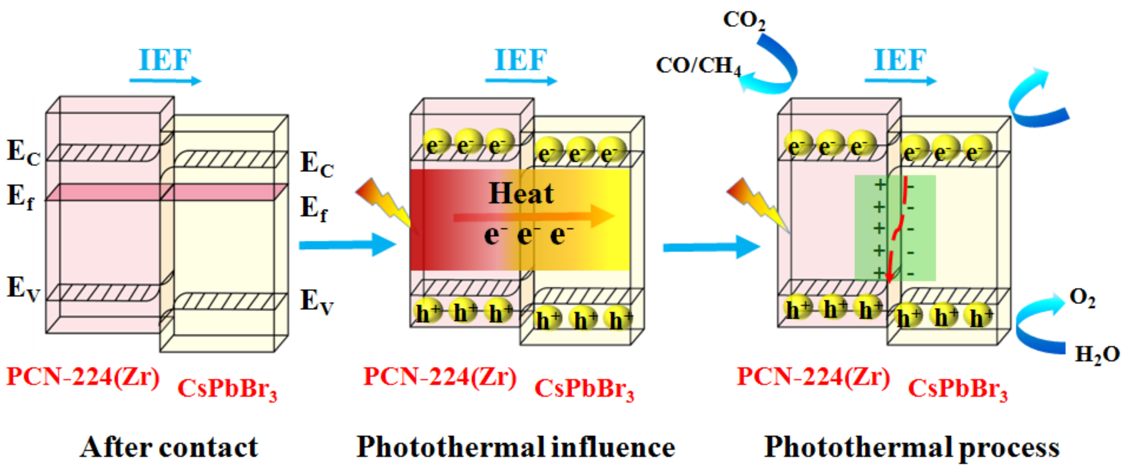

Fig.S18 The electron transfer model under photothermal coupled with photocatalytical process.

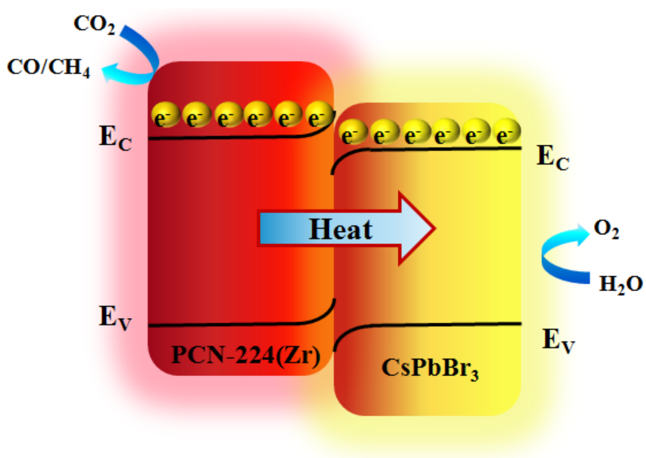

Fig.S19 The schematic view of photothermal effect on $CsPbBr_3$@PCN-224(Zr)-10 photocatalyst.

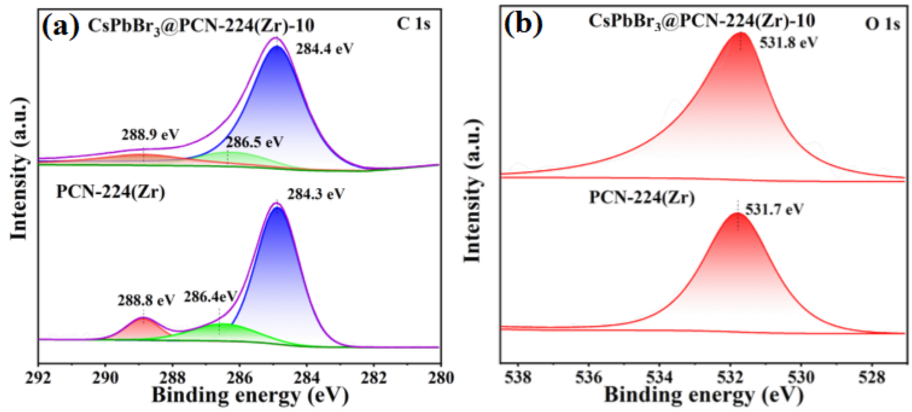

Fig.S20 The high-resolution XPS spectra of C 1s (a) and O 1s (b) over PCN-224(Zr) and $CsPbBr_3$@PCN-224(Zr)-10 composite.

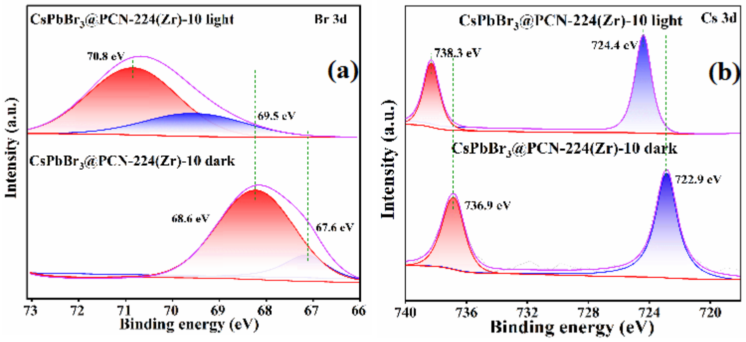

Fig.S21 The in situ XPS spectra of Br 3d (a) and Cs 3d (b) over $CsPbBr_3$@PCN-224(Zr)-10 composite with/without light irradiation.

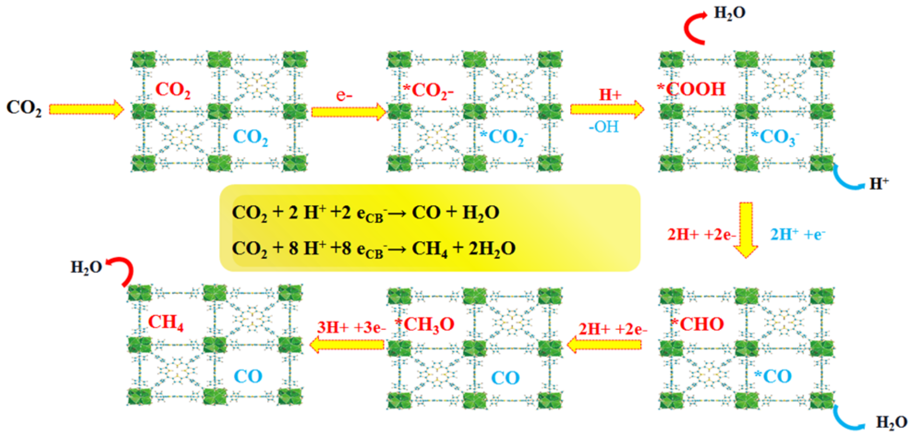

Fig.S22 The proposed mechanism of photocatalytic CO_2RR process.

3. Supplementary Tables

Table S1. The fitted internal resistance (R_s) and charge transfer resistance (R_{ct}) from the Nyquist plots.

Catalysts	$CsPbBr_3$ QDs		PCN-224(Zr)		$CsPbBr_3$@PCN-224(Zr)-5		$CsPbBr_3$@PCN-224(Zr)-10		$CsPbBr_3$@PCN-224(Zr)-15	
	light	dark	light	dark	light	dark	light	dark	light	dark
R_s (Ω)	361.7	394.4	116.1	299.6	106.9	203.3	98.5	136.2	130.3	228.4
R_{ct} (Ω)	3074	3590	1124	1616	324	838.9	278.2	791.4	325.8	923.3

Table S2. Summary of the photocatalytic CO_2RR performance under vis-NIR irradiation for 4 h over different photocatalysts in this paper.

Photocatalysts	**CO (4 h)** (μmol g^{-1})	**CH_4 (4 h)** (μmol g^{-1})	**CO efficiency** (μmol g^{-1} h^{-1})	**CH_4 efficiency** (μmol g^{-1} h^{-1})	**$R_{electron}$** (μmol g^{-1} h^{-1})
$CsPbBr_3$ QDs	60.1	5.0	15.03	1.25	40.06
PCN-224(Zr)	150.6	13.9	37.65	3.475	103.1

$CsPbBr_3$@PCN-224(Zr)-5	200.5	8.8	50.125	2.2	117.85
$CsPbBr_3$@PCN-224(Zr)-10	295.4	15.2	73.85	3.9	178.9
$CsPbBr_3$@PCN-224(Zr)-15	181.1	13.3	45.275	3.325	117.15

Table S3 Comparison of the photocatalytic CO_2 reduction over related photocatalysts.

Photocatalyst	Condition	Light	Product ($\mu mol\ g^{-1}$)		$R_{electron}$ ($\mu mol\ g^{-1}\ h^{-1}$)[a]	Ref.
			CO	CH_4		
M@C-Br	CO_2/H_2O, 4 h	300 W Xe lamp (320-780 nm)	106.35	15.51	85.0	2023
$CsPbBr_3$/UiO-66(NH_2)	EA/H_2O, 12h	300 W Xe lamp (420-800 nm)	98.57	3.08	18.48	1287
3-RhB@Zr-MOF	H_2O, 4 h	300 W Xe lamp (400-780 nm)	10.27	-	5.14	334
$Co_{2\%}$@$CsPbBr_3$@Cs_4PbBr_6	H_2O, 20 h	300 W Xe lamp (400-780 nm)	239	7.8	27.02	4769
CTU/0.6TiO_2	H_2O, 1 h	300 W Xe lamp (>300 nm)	31.32	0.148	63.82	926
WO_3/$CsPbBr_3$/ZIF-67	CO_2/H_2O, 3 h	150 W Xe lamp (>300 nm)	99.38	1.49	70.22	1550
UiO-68-OCH_3	TEOA, 50 ^oC, 6 h	300 W Xe lamp (400-780 nm)	118.1	-	19.69	8221
$CsPbBr_3$@ZIF-67	CO_2/H_2O, 3 h	100 W Xe lamp (400-780 nm)	2.30	10.54	29.63	2656
NMF/CPB-NWS	EA/H_2O, 3 h	300 W Xe lamp (420-780 nm)	320.4	-	160.2	120411
Zr-MOF@TP-TA	CO_2/H_2O,8 h	300 W Xe lamp (320-780 nm)	2.504	0.2	0.83	137011
$MAPbI_3$@PCN-221($Fe_{0.2}$)	EA/H_2O, 25 h	300 W Xe lamp (400-800 nm)	104	325	112.3	9491
CPB@Cu-TCPP-20	CH_3CN, 4 h	300 W Xe lamp (420-800 nm)	287.1	3.25	150.1	3192
$CsPbBr_3$@PCN-224(Zr)-10	CH_3CN, 4 h	300 W Xe lamp (420-800 nm)	295.4	15.3	178.2	This work

[a]$R_{electron}$ is the rate of total electron consumption for the reduced product.

Table S4 The fitted parameters of time-resolved PL curves of five photocatalysts.

Photocatalysts	**τ_1 [ns]**	**τ_2[ns]**	**τ_{ave} [ns]**
$CsPbBr_3$ QDs	2.1	16.47	15.9
PCN-224(Zr)	7.52	6.03	6.03
$CsPbBr_3$@PCN-224(Zr)-5	1.20	5.37	5.37
$CsPbBr_3$@PCN-224(Zr)-10	0.64	1.56	2.18
$CsPbBr_3$@PCN-224(Zr)-15	3.92	0.51	3.75

4. References

[1] J. Wang, Z. Dai, L. Wang, D. Zhang, Y. Wang, J. Li, F. Zhou, J. Huang, A Z-Scheme heterojunction of porphyrin-based core-shell Zr-MOF@Pro-COF-Br hybrid materials for efficient visible-light-driven CO_2 reduction, J. Mater. Chem. A, 11 (2023) 2023-2030.

[2] S. Wan, M. Ou, Q. Zhong, X. Wang, Perovskite-type $CsPbBr_3$ quantum dots/UiO-66(NH_2) nanojunction as efficient visible-light-driven photocatalyst for CO_2 reduction, Chem. Eng. J., 358 (2019) 1287-1295.

[3] O.-Y. Yang, X.-J. Gao, G.-D. Qi, Y. Wang, W.-W. Dong, Z.-F. Tian, J. Zhao, D.-S. Li, Q. Zhang, Dye-Anchoring Strategy with a Metal–Organic Framework for a Highly Efficient Visible-Light-Driven Photocatalytic CO_2 Reduction through the Solid–Gas Mode, ACS Appl. Energy Mater., 6(1) (2022) 334-341.

[4] Y.-F. Mu, W. Zhang, X.-X. Guo, G.-X. Dong, M. Zhang, T.-B. Lu, Water-Tolerant Lead Halide Perovskite Nanocrystals as Efficient Photocatalysts for Visible-Light-Driven CO_2 Reduction in Pure Water, ChemSusChem, 12(21) (2019) 4769-4774.

[5] L. Wang, P. Jin, S. Duan, H. She, J. Huang, Q. Wang, In-situ incorporation of Copper (II) porphyrin functionalized zirconium MOF and TiO_2 for efficient photocatalytic CO_2 reduction, Sci. Bull., 64(13) (2019) 926-933.

[6] Y.-J. Dong, Y. Jiang, J.-F. Liao, H.-Y. Chen, D.-B. Kuang, C.-Y. Su, Construction of a ternary WO_3/$CsPbBr_3$/ZIF-67 heterostructure for enhanced photocatalytic carbon dioxide reduction, Sci. Chin. Mater., 65(6) (2022) 1550-1559.

[7] Y.-P. Wei, Y. Liu, F. Guo, X.-Y. Dao, W.-Y. Sun, Different functional group modified zirconium frameworks for the photocatalytic reduction of carbon dioxide, Dalton Trans., 2019, 48(23), 8221-8226.

[8] Z.-C. Kong, J.-F. Liao, Y.-J. Dong, Y.-F. Xu, H.-Y. Chen, D.-B. Kuang, and C.-Y. Su, Core@Shell $CsPbBr_3$@Zeolitic Imidazolate Framework Nanocomposite for Efficient Photocatalytic CO_2 Reduction, ACS Energy Lett. 3 (2018) 2656−2662.

[9] Y. Xi, X. Zhang, Y. Shen, W. Dong, Z. Fan, K. Wang, S. Zhong, S. Bai, Aspect ratio dependent photocatalytic enhancement of $CsPbBr_3$ in CO_2 reduction with two dimensional metal organic framework as a cocatalyst, Appl. Catal. B: Environ. 297 (2021) 120411.

[10] L. Wang, J. Mao, G. Huang, Y. Zhang, J. Huang, H. She, C. Liu, H. Liu, Q. Wang, Configuration of hetero-framework via integrating MOF and triazine-containing COF for charge-transfer promotion in photocatalytic CO_2 reduction, Chem. Eng. J., 446 (2022) 137011.

[11] L.-Y. Wu, Y.-F. Mu, X.-X. Guo, W. Zhang, Z.-M. Zhang, M. Zhang, T.-B. Lu, Encapsulating Perovskite Quantum Dots in Iron-Based Metal–Organic Frameworks (MOFs) for Efficient Photocatalytic CO_2 Reduction, Angew. Chem. Int. Ed. 55(28), 9491-9495.

[12] N. Zhang, J.-J. Li, Y. Li, H. Wang, J.-Y. Zhang, Y. Liu, Y.-Z. Fang, Z. Liu and M. Zhou, Visible-light driven boosting electron-hole separation in $CsPbBr_3$ QDs@2D Cu-TCPP heterojunction and the efficient photoreduction of CO_2, J. Colloid Interface

Sci., 608 (2022) 3192-3203.